Traffic & Transportation

Bandwidth-Aware Event-Triggered Adaptive DMPC for Vehicle Platoon Control

Yiming SONG[1], Hongtao YE[2], Wenguang LUO[3], Xiaohua ZHOU[4], Jiayan WEN[5]

Original Scientific Paper
Submitted: 1 Aug 2025
Accepted: 4 Nov 2025
Published: 29 June 2026

[1] soyiming@163.com, School of Automation, Guangxi University of Science and Technology, Liuzhou, China
[2] Corresponding author, yehongtao@126.com, School of Automation, Guangxi University of Science and Technology, Liuzhou, China; Guangxi Key Laboratory of Automobile Components and Vehicle Technology, Guangxi University of Science and Technology, Liuzhou, China
[3] wgluo@gxust.edu.cn, School of Automation, Guangxi University of Science and Technology, Liuzhou, China
[4] zhxh76@126.com, School of Automation, Guangxi University of Science and Technology, Liuzhou, China
[5] wenjiayan2012@126.com, Guangxi Key Laboratory of Automobile Components and Vehicle Technology, Guangxi University of Science and Technology, Liuzhou, China

This work is licensed under a Creative Commons Attribution 4.0 International Licence.

Publisher:
Faculty of Transport and Traffic Sciences, University of Zagreb

ABSTRACT
Self-driving vehicle platoons offer promising improvements in traffic efficiency and safety. However, their deployment is hindered by limited communication bandwidth and computational constraints in distributed control systems. This paper presents a bandwidth-aware event-triggered adaptive distributed model predictive control (DMPC) method. Firstly, to mitigate resource waste from frequent communications under bandwidth-constrained conditions in conventional DMPC, a bandwidth-aware event-triggered mechanism is designed based on a sigmoid threshold function of vehicle state errors. This mechanism adjusts the triggering threshold according to bandwidth availability, thereby suppressing unnecessary transmissions while maintaining a balance between communication efficiency and control performance. Secondly, a dual-input fuzzy adaptive module is introduced to reduce the computational burden in vehicle platoon control. This module takes maximum position and velocity errors as inputs to tune the prediction horizon dynamically. Finally, numerical simulation results show that under high bandwidth usage, the proposed method reduces communication resource consumption to 57.3%, while decreasing the communication frequency by up to 15.7% compared with the existing method. Meanwhile, it decreases the controller's computational overhead by up to 20.45% relative to fixed-horizon DMPC. The proposed approach enhances both communication and computational efficiency, making it applicable for resource-constrained platoon control scenarios.

KEYWORDS
vehicle platoon; distributed model predictive control; event-triggered mechanism; bandwidth-aware; adaptive prediction horizon; fuzzy control.

1. INTRODUCTION

With the continued rise in vehicle ownership and rapid urban development, modern transportation systems are increasingly plagued by traffic congestion and elevated accident rates – issues that not only reduce travel efficiency but also pose a threat to public safety. Connected and automated vehicle (CAV) systems are widely recognised as an effective approach to addressing these challenges [1]. Vehicle platooning enables close-range coordination among vehicles, which has been shown to reduce traffic congestion, increase transportation safety and boost traffic efficiency [2–5]. Moreover, platoon driving can significantly reduce the burden on drivers and effectively prevent traffic accidents caused by human factors such as operational errors and driver fatigue,

thereby greatly improving road safety [6]. To realise these advantages, effective cooperative control strategies are required, especially those that can handle constraints (e.g. safety distance, communication limits) in distributed systems. DMPC is an optimal control strategy that decomposes a global optimisation problem into sub-problems for individual subsystems. It predicts future system states while handling constraints, solving local optimisation problems in real time to achieve cooperative control among multiple agents [7–8]. In vehicle platoon control, DMPC has been widely employed in related research due to its ability to explicitly handle constraints and perform online receding horizon optimisation. Additionally, its advantages of low communication overhead, high computational efficiency, strong fault tolerance and system scalability make it particularly suitable for platoon scenarios [9–12].

Prior research indicates that significant communication delays or packet losses can substantially impair the tracking performance of vehicle platoons. Given the limitations of communication resources, inter-vehicle data transmission should be managed adaptively to enhance communication efficiency. To reduce unnecessary inter-vehicle data transmission, researchers have investigated cooperative control of vehicle platoons from the perspectives of event-triggered mechanism (ETM) and communication data quantisation [13–19]. Bansal and Mukhija [13] tackled sensor faults and time-varying communication delays by designing a novel event-triggered strategy that employs actual fault values instead of expected values, thereby achieving both intra-platoon and string stability. Ge et al. [14] introduced a bandwidth-aware dynamic event-triggered mechanism that balances communication efficiency and formation control performance by dynamically adjusting trigger threshold parameters. Combined with distributed control, this integrated method ensures robust platoon tracking under unknown disturbances, effectively addressing the cooperative design problem under constrained bandwidth in vehicular networks. Han et al. [15] developed a bandwidth-aware transmission scheduling (BATS) mechanism to regulate communication based on bandwidth conditions. This mechanism was further integrated with an event-triggered distributed model predictive control (ET-DMPC) scheme to reduce the computational frequency of online optimisations. Zhang et al. [17] presented a fixed-time cooperative control strategy to address output constraints, event-triggered conditions and communication delays in high-order multi-agent systems. To further counteract communication delays, they also designed an event-triggered observer. Zhang et al. [18] proposed a sigmoid-like ETM secure cruise control strategy, where a dynamic threshold was employed to balance communication efficiency and robustness against cyberattacks. Xie et al. [19] introduced a sigmoid-based adaptive control method, which uses a hyperbolic tangent function to dynamically adjust the triggering threshold. This approach significantly improves the minimum inter-execution interval and prevents frequent triggering that could lead to network congestion.

In addition to communication-related challenges, the design of time-domain parameters in platoon control also affects performance. Most of the aforementioned controllers adopt fixed prediction and control horizons, which can significantly affect the control accuracy and stability of vehicle platoons. Fixed time horizons are often inadequate in responding to sudden state variations, making it difficult to dynamically adapt to changing platoon conditions, thereby resulting in reduced tracking accuracy and potential stability issues. To address these limitations, researchers have introduced adaptive control strategies to enable dynamic adjustment of time-domain parameters [20–24]. Lin et al. [20] proposed a fuzzy controller that adaptively adjusts the prediction horizon, thereby addressing the limitations of fixed MPC parameters and enhancing adaptability in complex scenarios. Liu et al. [22] designed a curvature-adaptive hierarchical MPC algorithm, where fuzzy logic is integrated into both MPC layers to dynamically adjust the prediction and control horizons based on heading error and vehicle speed, thereby improving system robustness and reducing computational burden. Wang et al. [23] introduced an adaptive ET-DMPC approach, where a time-domain reduction mechanism was designed to lower computational complexity.

Motivated by the preceding analysis, this study proposes an event-triggered adaptive DMPC strategy. The method combines a bandwidth-aware event-triggered mechanism with an adaptive time-domain parameter strategy. The primary contributions of this study are summarised as follows.

1) To address the communication bandwidth limitation in vehicle platoons, a bandwidth-aware event-triggered mechanism is proposed based on vehicle state errors and a sigmoid threshold function. A small platoon error leads to a lower triggering frequency. In contrast, a larger error makes the triggering condition easier to satisfy. It is also theoretically proven that the proposed design avoids Zeno behaviour.
2) A fuzzy adaptive module is developed that takes the maximum displacement and speed deviations of the platoon as inputs to dynamically tune the controller's prediction horizon. This design alleviates computational demands while maintaining stable platoon behaviour.

3) A Lyapunov function for the platoon system is constructed, and the asymptotic stability of the system under the proposed control strategy is rigorously proven. In addition, a theoretical condition ensuring platoon stability is established.

2. DESCRIPTION OF THE PROBLEM

This section establishes the discrete nonlinear dynamic model of the platoon vehicles. It introduces the communication topology and describes the geometric configuration of the platoon.

2.1 Nonlinear vehicle dynamics model

The longitudinal dynamics of a vehicle exhibit strong nonlinearity, and the main sources include the engine, transmission, quadratic aerodynamic drag and braking system. Accordingly, the vehicle platoon is modelled using a nonlinear longitudinal dynamic formulation, as shown in *Equation 1*.

$$\begin{cases} \dot{p}_i(t) = v_i(t) \\ \dfrac{\eta_{T,i}}{r_{w,i}} T_i(t) = m_i \dot{v}_i(t) + C_{A,i} v_i^2(t) + m_i g f_i, \quad i \in \mathcal{N} \\ \tau_i \dot{T}_i(t) + T_i(t) = T_{\mathrm{des},i}(t) \end{cases} \tag{1}$$

where $p_i(t)$, $v_i(t)$, $T_i(t)$ represent the position, speed and driving/braking torque of vehicle i, respectively. The index set is denoted as $\mathcal{N} = \{1,2,\cdots,N\}$. Each vehicle is characterised by its mass m_i, rolling resistance coefficient f_i and tire radius $r_{w,i}$. Aerodynamic drag is modelled using the coefficient $C_{A,i}$, and g denotes the gravitational constant. The mechanical efficiency of the driveline is represented by $\eta_{T,i}$, while τ_i represents the inertial lag in the longitudinal dynamics. The desired input signal $T_{des,i}(t)$ corresponds to the required traction or braking torque at time t, indicating the control effort applied to the powertrain.

The platoon state variables include the vehicle displacement, velocity and motor output torque, formulated as $x_i(t) = [p_i(t),\ v_i(t),\ T_i(t)]^T$. The control input is defined as $u_i(t) = T_i(t)$, which represents the output torque of the vehicle's motor. *Equation 2* is denoted as:

$$\begin{cases} \dot{x}_i = f(x_i(t), u_i(t)) \\ y_i = \gamma x_i \end{cases} \tag{2}$$

where $\gamma \in R^{2\times 3}$ is the output matrix, $\gamma = \begin{bmatrix} 1 & 0 & 0 \\ 0 & 1 & 0 \end{bmatrix}$.

The above equation is a continuous-time dynamics model. For practical control implementation, it is converted into a discrete-time model with a sampling interval of h. Specifically, *Equation 1* is discretised to obtain:

$$x_i(t+1) = \theta_i(x_i) + \psi_i \cdot u_i(t) \tag{3}$$

where $\theta_i = \begin{bmatrix} p_i(t) + v_i(t)h \\ v_i(t) + \frac{h}{m_i}\left(\frac{\eta_{T,i}}{r_{w,i}} T_i - C_{A,i} v_i^2(t) - m_i g f_i\right) \\ T_i(t) - \frac{1}{\tau_i} T_i(t) h \end{bmatrix}$, $\psi_i = \begin{bmatrix} 0 \\ 0 \\ \frac{1}{\tau_i} h \end{bmatrix}$.

2.2 Communication topology, platoon geometry and control objectives

Vehicle-to-vehicle (V2V) communication enables short-range data exchange, such as vehicle speed, among vehicles. The communication topology defines the information flow within the platoon and extends each vehicle's perception range – an accurate topology model is essential for formulating local optimisation problems in DMPC. As reported in [9], information exchange within a vehicle platoon is modelled as a directed graph $G = \{V, E\}$, where $V = \{0,1,2,\cdots,N\}$ defines the node set, and $E \subseteq V \times V$ characterises the communication links among vehicles. This work focuses on two representative topologies: predecessor-following (PF) and predecessor-leader following (PLF), which are commonly employed in practical platoon control scenarios. Other topologies, such as two-predecessors-following (TPF) and two-predecessors-leader-

following (TPLF), also exist but are not considered in this study. The corresponding communication topologies are shown in *Figure 1*.

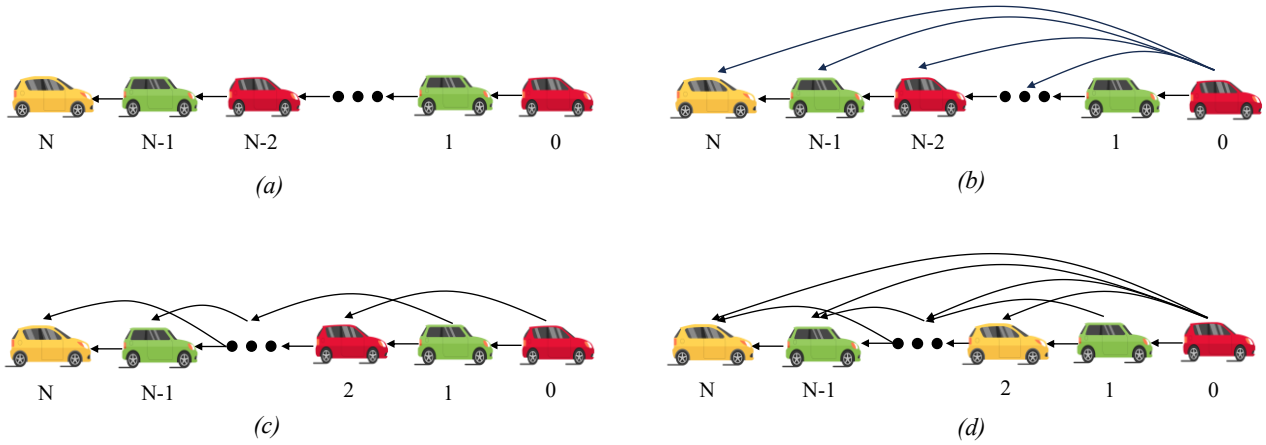

Figure 1 – Communication topology: a) PF; b) PLF; c) TPF; d) TPLF

The platoon geometric configuration in this study adopts a constant spacing strategy, that is:

$$d_{i-1,i} = d_0, i \in \mathcal{N} \tag{4}$$

where $d_{i-1,i} > 0$ is the desired distance between adjacent vehicles, specified by a positive constant d_0.

The control objective of the platoon is to synchronise the velocities of all follower vehicles with that of the leader and maintain the desired spacing, which can be formulated as:

$$\begin{cases} \lim\limits_{t\to\infty} \| v_i(t) - v_0(t) \| = 0 \\ \lim\limits_{t\to\infty} \| p_{i-1}(t) - p_i(t) - d_{i-1,i} \| = 0 \quad i \in \mathcal{N} \end{cases} \tag{5}$$

where v_0 denotes the velocity of the leader vehicle.

3. BANDWIDTH-AWARE EVENT-TRIGGERED ADAPTIVE DMPC STRATEGY

An event-triggered mechanism is proposed based on the nonlinear vehicle platoon model, considering both bandwidth variations and platoon states. It ensures control performance while reducing unnecessary communication and is proven free of Zeno behaviour. Since the prediction horizon N_p and control horizon N_c critically affect DMPC performance, an algorithm is designed to adaptively optimise N_p.

3.1 Bandwidth-aware event-triggered mechanism

The information flow topology of the platoon determines how member vehicles convey their state information to neighbouring vehicles. To improve platoon control performance, a well-structured information flow topology and an efficient transmission mechanism are essential. This study assumes ideal communication conditions where each vehicle reliably receives the required state information. However, given the constraints of limited bandwidth, continuous broadcasting is inefficient. To address this, a bandwidth-aware event-triggered strategy is proposed, which incorporates a sigmoid-based nonlinear threshold modulation to regulate transmission frequency. The framework of this mechanism is shown in *Figure 2*. Here, $\alpha \in [0,1]$ is a preset modelling parameter that characterises different bandwidth scenarios. It is not based on real-time network load measurement but serves to simulate varying bandwidth conditions in the event-triggered mechanism.

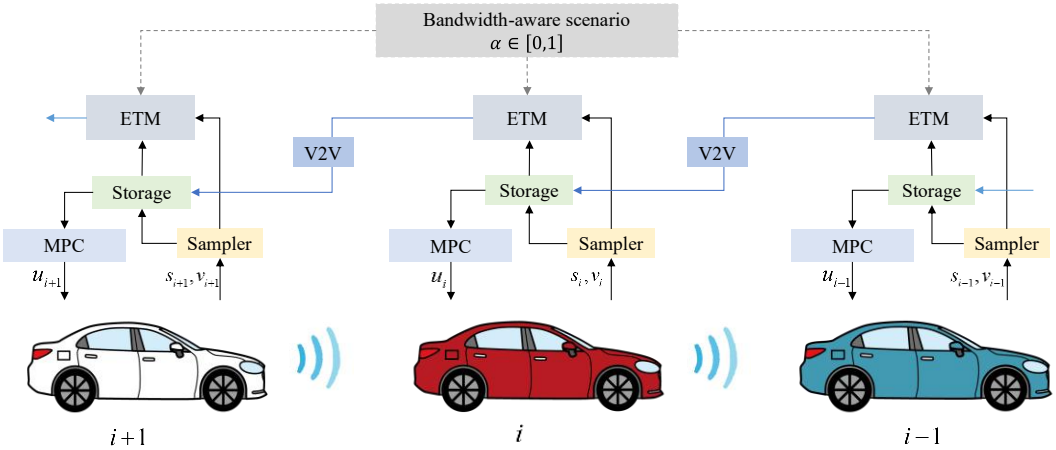

Figure 2 – Framework of the bandwidth-aware event-triggered mechanism

In the event-triggered DMPC structure, a triggering mechanism is constructed in the feedback loop of each vehicle and decides whether to send the vehicle's state information at the current moment to its neighbours. When the triggering condition is fulfilled, the corresponding state data are communicated. The triggering condition in the bandwidth-aware event triggering mechanism is denoted as:

$$t_{k+1}^{i} = inf\{t > t_k^i \mid F_i(t) > 0\} \tag{6}$$

where $F_i(t)$ is denoted as:

$$F_i(t) = \left\|\Phi^{\frac{1}{2}} e_i(t)\right\|^2 - \sigma_\alpha(t)\left\|\Phi^{\frac{1}{2}} \varrho(t)\right\|^2 \tag{7}$$

where $e_i(t) = \begin{bmatrix} p_i(t_k^i) + p_{i-1}(t) - d - 2\cdot p_i(t) \\ v_i(t_k^i) + v_{i-1}(t) - 2\cdot v_i(t) \end{bmatrix}$, $\varrho(t) = \begin{bmatrix} ds_i / \left(p_i(t_k^i) - p_{i-1}(t)\right) \\ ds_i / \left(v_i(t_k^i) - v_{i-1}(t)\right) \end{bmatrix}$. $p_i(t)$ and $v_i(t)$ denote the current sampled position and velocity of vehicle i. $p_i(t_k^i)$ and $v_i(t_k^i)$ represent the position and velocity of vehicle i at its last triggering instant. $e_i(t)$ is the error term, which includes the deviation between the state of vehicle i at its last transmission instant and its current state, as well as the deviation between its current state and the desired state of the preceding vehicle $i-1$. The term $\varrho(t)$ represents the magnitude of state variation; as the tracking error and state variation within the vehicle platoon increase, the triggering condition is more likely to be satisfied. Φ is a non-negative weighting matrix, and $ds_i \in (0,1)$ is a conditioning factor used to regulate the data transmission frequency within the platoon.

$\sigma_\alpha(t)$ is the bandwidth-aware dynamic parameter denoted as:

$$\sigma_\alpha(t) = \alpha\eta_i(t) + (1-\alpha)\varsigma_i(t) \tag{8}$$

Here, $\alpha \in [0,1]$ is the bandwidth state acknowledgement parameter, whose relationship with the bandwidth state is shown in *Table 1*. Under heavy bandwidth usage conditions (i.e. $\alpha = 0$), only the dynamic parameter $\varsigma_i(t)$, characterised as a monotonically non-decreasing and upper-bounded function, remains active. This indicates that less vehicle state information is transmitted over the network. Conversely, in a network with idle bandwidth usage (i.e. $\alpha = 1$), only the dynamic parameter $\eta_i(t)$, which is monotonically non-increasing and bounded below, takes effect, allowing more vehicle state information to be transmitted.

Table 1 – Relationship between α and bandwidth states

α values	**bandwidth states**
$\alpha = 0$	busy
$\alpha \in (0,1)$	moderate
$\alpha = 1$	idle

In *Equation 8*, $\eta_i(t)$ and $\varsigma_i(t)$ denote dynamic threshold parameters that are updated at each sampling instant based on the following update rules.

$$\eta_i(t+1) = \frac{\eta_i(t)}{1+\beta_1\eta_i(t)\left\|\Phi^{\frac{1}{2}}e_i(t)\right\|^2} \tag{9}$$

$$\varsigma_i(t+1) = \frac{\varsigma_i(t)\left\|\Phi^{\frac{1}{2}}e_i(t)\right\|^2 + \beta_2\bar{\varsigma}_i}{\beta_2 + \left\|\Phi^{\frac{1}{2}}e_i(t)\right\|^2} \tag{10}$$

where the initial conditions: $\beta_1 \geq 0$, $\beta_2 \geq 0$, $0 \leq \eta_i(0) \leq \bar{\eta}_i \leq \varsigma_i(0) \leq \bar{\varsigma}_i$, $\bar{\eta}_i \in [0, \bar{\varsigma}_i)$, $\bar{\varsigma}_i \in [0,1)$ are prescribed scalars.

3.2 Event-triggered mechanism based on sigmoid threshold function

To reduce unnecessary triggering when the state error is small, this subsection introduces a nonlinear thresholding method based on the sigmoid function.

Based on *Equations 6 and 7*, the sigmoid ETM strategy is formulated as:

$$t_{k+1}^i = inf\left\{t > t_k^i \mid \tilde{\delta}(t)\left\|\Phi^{\frac{1}{2}}e_i(t)\right\|^2 - \sigma_\alpha(t)\left\|\Phi^{\frac{1}{2}}\varrho(t)\right\|^2 > 0\right\} \tag{11}$$

where $\tilde{\delta}(t) = \frac{1}{1+e^{\left(-\kappa\times\left(\sqrt{\|e_i(t)\|}-\varepsilon\right)\right)}}$; $\kappa > 0$ is the slope parameter; $\varepsilon > 0$ is the threshold. The sigmoid function $\tilde{\delta}(t)$, used to adjust the event-triggering threshold, has the following mathematical characteristics.

1) $\tilde{\delta}(t)$ is a function that increases monotonically with $\|e_i(t)\|$.
2) The parameter takes values within the interval $\left(\frac{1}{1+e^{\kappa\varepsilon}}, 1\right)$.

Parameter $\tilde{\delta}(t)$ is adaptively adjusted according to the variation in the state error $e_i(t)$. When the system approaches a stable state, i.e. $\|e_i(t)\|$ tends to zero, the event-triggered condition in *Equation 11* yields a smaller value of $\tilde{\delta}(t)$, indicating that fewer data transmissions are required over the network. Conversely, as $\|e_i(t)\|$ increases, suggesting a deviation from the stable state, a larger value of $\tilde{\delta}(t)$ is required to satisfy the trigger condition, thereby enabling more data to be transmitted.

3.3 Exclusion of Zeno behaviour

The event-triggered control scheme must exclude Zeno behaviour, which refers to the occurrence of infinitely many triggering events within a finite time interval – a scenario that is impractical for physical controllers. To validate the practical feasibility of the bandwidth-aware sigmoid event-triggering mechanism, it is necessary to establish a positive minimum threshold on the time gap between triggering events. This ensures the effective exclusion of Zeno behaviour.

The vehicle platoon in this study is modelled using a nonlinear discrete-time system. According to *Equation 11*, the sampled data packet $\left(t_k^i, x_i(t_k^i)\right)$ is transmitted only when the triggering function exceeds zero. This implies that the set of triggering instants $\left\{t_0^i, t_1^i, t_2^i, \cdots\right\}$ is a subset of the sampling time set $\{0, h, 2h, \cdots\}$. In this study, the minimum event triggering interval $T_{\min}^i$ is:

$$T_{\min}^i \triangleq \min\left\{t - t_k^i\right\} \geq h > 0 \tag{12}$$

It is shown that the designed event-triggered mechanism ensures a strictly positive lower bound for the minimum triggering interval, thereby excluding Zeno behaviour.

3.4 Adaptive time-horizon DMPC optimisation strategy

This section proposes an adaptive time-horizon optimisation strategy for DMPC, utilising a fuzzy control approach to adjust the time horizon adaptively, thereby achieving a fuzzy adaptive prediction horizon N_p. In this work, N_p and N_c are set to be equal (i.e. $N_p = N_c$). This configuration simplifies the design and

computation of time-domain parameters, ensures consistency between the control inputs and the predicted outputs of the system in the time scale, and reduces the complexity of parameter scheduling. Therefore, only the prediction horizon N_p requires adaptive optimisation.

The fuzzy control algorithm uses the maximum position and velocity errors of the platoon as inputs and the variation of the DMPC prediction horizon as the output. This enables real-time optimisation of the prediction horizon during vehicle following, thereby achieving a dynamic balance between computational load and tracking performance: the prediction horizon is automatically extended when errors increase to improve control accuracy, and shortened when errors decrease to reduce computational burden.

The formula for the maximum position error in the vehicle platoon is given by:

$$\bar{e}_p = \|p_{i-1} - p_i - d_{i-1,i}\|_\infty, i \in \mathcal{N} \tag{13}$$

The formula for the maximum velocity error in the vehicle platoon is given by:

$$\bar{e}_v = \|v_{i-1} - v_i\|_\infty, i \in \mathcal{N} \tag{14}$$

The input variables are classified into five linguistic levels (VL, L, M, H, VH), and the output variable into seven levels (VS, S, MS, M, ML, L, VL). In the fuzzy controller, triangular membership functions are used for inputs due to their simplicity and accuracy, whereas Gaussian membership functions are applied to outputs to suppress jitter and enhance smoothness. *Figure 3* illustrates the membership function distributions. This input-output combination effectively balances computational efficiency and control smoothness.

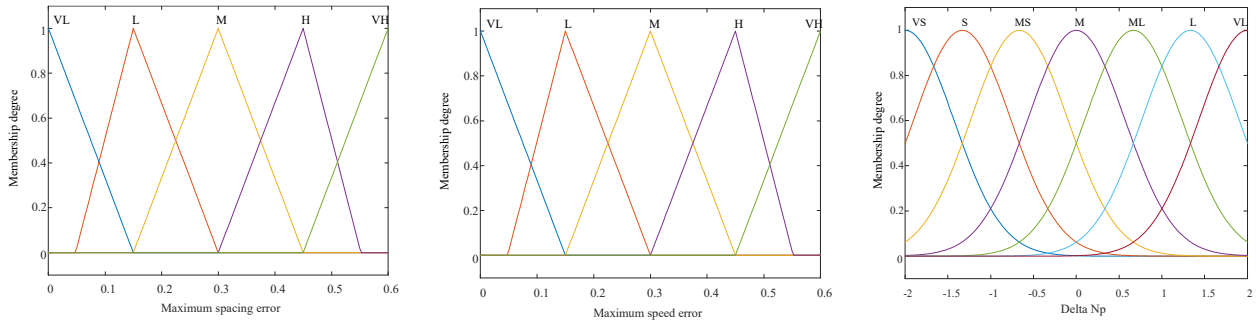

(a) *(b)* *(c)*

Figure 3 – Membership functions of the fuzzy controller inputs and output: a) Maximum position error; b) Maximum velocity error; c) Prediction horizon

Table 2 – Fuzzy rule table

$\bar{e}_p$	$\bar{e}_v$				
	VL	**L**	**M**	**H**	**VH**
VL	MS	M	ML	ML	VL
L	M	M	ML	L	VL
M	M	L	VL	VL	VL
H	L	L	VL	VL	VL
VH	VL	VL	VL	VL	VL

According to the prediction horizon optimisation strategy, the fuzzy rules are formulated according to the following principles: a smaller $\bar{e}_p$ and $\bar{e}_v$ result in a reduced N_p, whereas larger values extend N_p; other cases are addressed through qualitative analysis based on expert knowledge. The designed fuzzy rule set is presented in *Table 2*, and the input-output response surface of the fuzzy controller is illustrated in *Figure 4*.

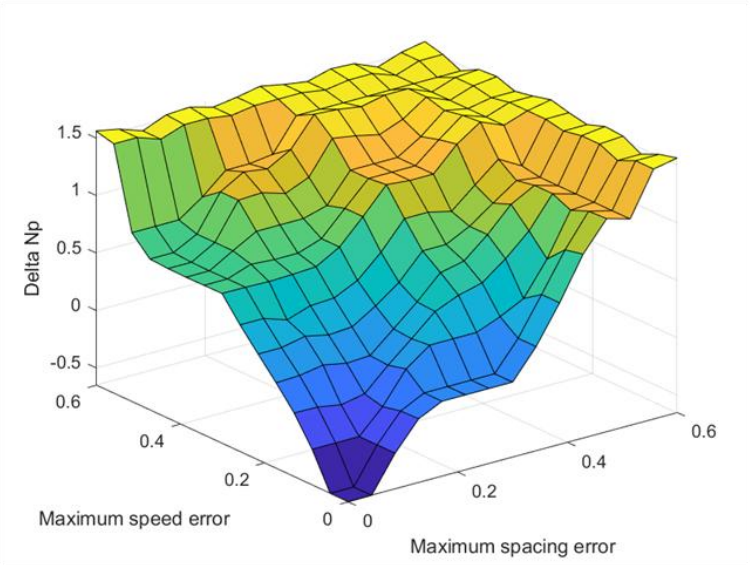

Figure 4 – Response surfaces of the fuzzy controller's inputs and outputs

Through fuzzy inference on the maximum position error and maximum velocity error, the centre of gravity method is employed for defuzzification to obtain the variation of the prediction horizon, denoted as ΔN_p. Based on the previous prediction horizon N_p^k , the new prediction horizon N_p^{k+1} is derived using *Equation 15*.

$$N_p^{k+1} = N_p^k + \Delta N_p \tag{15}$$

4. DESIGN OF DMPC SYSTEM

This section introduces a DMPC control framework that integrates PF and PLF communication topologies. Using a nonlinear model of vehicle longitudinal dynamics, a sub-prediction optimisation problem is formulated for each vehicle in the heterogeneous platoon. The transmitted information is then used to optimise the cost function, from which the optimal control inputs are determined.

4.1 Controller system design

At a given time t, $X(t) = [x_1^T(t), x_2^T(t), \cdots, x_N^T(t)]^T \in \mathbb{R}^{3N}$,$Y(t) = [y_1^T(t), y_2^T(t), y_N^T(t)]^T \in \mathbb{R}^{2N}$ and $U(t) = [u_1(t), u_2(t), \cdots u_N(t)]^T \in \mathbb{R}^{2N}$ are the platoon's collective state, output and input vectors platoon. The overall platoon dynamics are governed by:

$$\begin{cases} X(t+1) = \Theta(X(t)) + \Psi \cdot U(t) \\ Y(t) = \Gamma X(t) \end{cases} \tag{16}$$

where $\Theta = [\theta_1(x_1)^T, \theta_2(x_2)^T, \cdots, \theta_N(x_N)^T]^T$, $\psi = diag\{\psi_1, \psi_2, \cdots, \psi_N\}$ and $\Gamma = diag\{\gamma_1, \gamma_2, \cdots, \gamma_N\}$. Using *Equation 16* as the system's predictive model, the system states and outputs over the future N_p steps are predicted based on the current system state and the control inputs within the finite future horizon. The control input and output state quantities of the following vehicle are now defined and each variable contains three types. All variables are shown in *Table 3*.

Table 3 – Definitions of control input and output variables

Symbol	Name	Symbol	Name
$u_i^p(k\|t)$	Predicted control input	$y_i^p(k\|t)$	Predicted state output
$u_i^*(k\|t)$	Optimal predicted control input	$y_i^*(k\|t)$	Optimal predicted output
$u_i^a(k\|t)$	Assumed control input	$y_i^a(k\|t)$	Assumed state output

The local optimisation problem for vehicle i is defined as:

$$\min_{U_i} f_i\left(y_i^p(\cdot\mid t), u_i^p(\cdot\mid t), y_i^a(\cdot\mid t), y_{-i}^a(\cdot\mid t)\right) = \sum_{k=0}^{N_p-1} l_i\left(\mathbf{y}_i^p(k\mid t), u_i^p(k\mid t), \mathbf{y}_i^a(k\mid t), \mathbf{y}_{-i}^a(k\mid t)\right) \tag{17}$$

$$s.t. \begin{cases} \dot{x}_i^P(k+1\mid t) = \theta_i\left(x_i^P(k\mid t)\right) + \psi_i \cdot u_i^P(k\mid t) \\ y_i^P(k\mid t) = \gamma x_i^P(k\mid t), \qquad k = 0,\cdots,N_p-1 \\ x_i^P(0\mid t) = x_i(t) \end{cases} \tag{18}$$

$$u_i^p(k\mid t) \in u \tag{19}$$

$$\boldsymbol{y}_i^p(N_p|t) = \frac{1}{|\mathbb{I}_i|}\sum_{j\in\mathbb{I}_i}\left(\boldsymbol{y}_j^a(N_p|t) - \tilde{\boldsymbol{d}}_{j,i}\right) \tag{20}$$

$$T_i^p(N_p|t) = h_i\left(v_i^p(N_p|t)\right) \tag{21}$$

where $U_i = \left[u_i^p(0\mid t), u_i^p(1\mid t), \cdots, u_i^p\left(N_p-1\mid t\right)\right]^T$ denotes the sequence of predicted control inputs to be optimised. $|\mathbb{I}_i|$ indicates the number of elements in the set $\mathbb{I}_i = \mathbb{N}_i \cup \mathbb{P}_i$, $\tilde{d}_{j,i} = [-(j-i)d_0, 0]^T$ represents the state deviation between nodes; and h_i is the ego vehicle's velocity function, which balances aerodynamic drag and road friction resistance. *Equation 18* describes the dynamic constraints within the prediction horizon; *Equation 19* imposes amplitude constraints on the control input, *Equations 20 and 21* are equality constraints at the prediction terminal.

The vehicle's cost function is formulated as follows:

$$\begin{aligned} l_i\left(y_i^p(k\mid t), u_i^p(k\mid t), y_i^a(k\mid t), y_{-i}^a(k\mid t)\right) &= \left\|\left(y_i^p(k\mid t) - y_{i,\mathrm{des}}(k\mid t)\right)\right\|_{Q_i}^2 + \left\|\left(u_i^p(k\mid t) - h_i\left(v_i^p(k\mid t)\right)\right)\right\|_{R_i}^2 \\ &+ \left\|\left(y_i^p(k\mid t) - y_i^a(k\mid t)\right)\right\|_{F_i}^2 + \sum_{j\in\mathbb{N}_i}\left\|\left(y_i^p(k\mid t) - y_j^a(k\mid t) - \tilde{d}_{i,j}\right)\right\|_{G_i}^2 \end{aligned} \tag{22}$$

where Q_i, R_i , F_i and G_i are weighting coefficients in the cost function, all assumed to be symmetric positive semi-definite matrices. When $Q_i > 0$, vehicle node i can access information from the leading vehicle; otherwise, $Q_i = 0$. $R_i \geq 0$ reflects the penalty on acceleration and deceleration behaviours, characterising the node's preference for constant speed. $F_i \geq 0$ indicates that the vehicle node i should adhere to the trajectories assumed by other vehicle nodes. $G_i \geq 0$ reflects that vehicle node i should, as much as possible, follow the assumed trajectories of its neighbouring vehicle nodes.

4.2 Algorithm of DMPC

Equation 16 formulates the optimisation problem for vehicle i, which leverages local information from neighbouring vehicles to achieve global optimisation. In DMPC, each vehicle synchronously solves its own optimisation problem based on its own and its neighbours' assumed states. Since real-time optimisation results at the current triggering instant t_k^i cannot be immediately shared, the assumed states are predicted based on the neighbours' optimal control states from the previous time step t_{k-1}^i. This approach helps avoid coordination issues caused by communication delays. The procedure of the algorithm is outlined below.

1) The platoon at $t = 0$ is initialised with a constant velocity. Accordingly, the input and output sequences of vehicle i are given by:

$$\begin{cases} u_i^a(k\mid 0) = f(v_i(0)), k = 0,1,\cdots,N_p-1 \\ y_i^a(k+1\mid 0) = y_i^p(k+1\mid 0), k = 0,1,\cdots,N_p-1 \end{cases} \tag{23}$$

where $\dot{x}_i^p(k+1\mid 0) = \theta_i\left(x_i^p(k\mid 0)\right) + \psi_i \cdot u_i^a(k\mid 0)$, $\gamma_i^p(k\mid 0) = \gamma x_i^p(k\mid 0)$, $x_i^p(k\mid 0) = x_i(k\mid 0)$, $k = 0,1,\cdots,N_p-1$.

2) At the triggering instant t_k^i, vehicle node i employs its own predicted output $y_i^a(k \mid t_k^i)$, the predicted outputs of its neighbours $y_{-i}^a(k \mid t_k^i)$, and the reference trajectory $y_{i,des}(k \mid t_k^i)$ from the lead vehicle.
3) The optimal control input $u_i^*(0|t_k^i)$ is applied to each vehicle node to compute the optimal state sequence over the prediction horizon.

$$\begin{cases} x_i^*(k+1 \mid t_k^i) = \theta_i(x_i^*(k \mid t_k^i)) + \psi_i \cdot u_i^*(k \mid t_k^i) \\ x_i^*(0 \mid t_k^i) = x_i(t_k^i) \end{cases} \tag{24}$$

4) Calculate the assumed input sequence and its associated assumed output sequence for the prediction step.

$$u_i^a(k \mid t_{k+1}^i) = \begin{cases} u_i^*(k+1 \mid t_k^i), & k = 0,1,\cdots,N_p-2 \\ h_i\left(v_i^*(N_p \mid t_k^i)\right), & k = N_p-1 \end{cases} \tag{25}$$

$$\begin{cases} x_i^a(k+1 \mid t_{k+1}^i) & = \theta_i(x_i^a(k \mid t_{k+1}^i)) + \psi_i \cdot u_i^a(k \mid t_{k+1}^i) \\ y_i^a(k+1 \mid t_{k+1}^i) & = \gamma \cdot x_i^a(k+1 \mid t_{k+1}^i), k = 0,1,\cdots,N_p-1 \end{cases} \tag{26}$$

5) Through V2V communication, the assumed output state $y_i^a\left(k \mid t_{k+1}^i\right)$ is transmitted to neighbouring nodes, while the assumed output trajectories $y_{-i}^a(k \mid t_{k+1}^i)$ from these neighbouring nodes are received. Additionally, if connected to the lead vehicle, the reference trajectory $y_{i,des}(k \mid t_{k+1}^i)$ is obtained to enable local information sharing within the platoon.

4.3 Stability analysis

A Lyapunov-based stability analysis is conducted by constructing a function that sums the individual cost functions of all following vehicles. By demonstrating that this function is monotonically non-increasing over time, the platoon is proven to be asymptotically stable. The optimal cost for the entire platoon at the triggering instant t_k^i is defined as:

$$V(t_k) = \sum_{i=1}^{N} J_i^*(t_k^i) \tag{27}$$

where $J_i^*(t_k^i)$ denotes the optimal local performance index obtained by vehicle node i at time t_k^i:

$$V_i(t_k^i) = J_i^*(t_k^i) \tag{28}$$

Theorem 4.1: For the optimisation problem defined in *Equation 22* of the DMPC framework, once the predicted terminal state of a node coincides with the desired reference state, the one-step cost reduction follows the inequality below:

$$V_i(t_{k+1}^i) - V_i(t_k^i) \le -l_i(\cdot) + \varepsilon_i \tag{29}$$

where $l_i(\cdot)$ denotes the stage cost evaluated at time t_k^i, $\varepsilon_i = \sum_{k=1}^{N_p} \left\{ \sum_{j \in \mathbb{N}_i} \left\| y_j^*(k \mid t_k^i) - y_j^a(k \mid t_k^i) \right\|_{G_i}^2 - \left\| y_i^*(k \mid t_k^i) - y_i^a(k \mid t_k^i) \right\|_{F_i}^2 \right\}$.

Proof: At the subsequent triggering instant t_{k+1}^i, the optimal cost is given by:

$$\begin{aligned} V_i(t_{k+1}^i) &\le J_i\left(y_i^p(\cdot \mid t_{k+1}^i), u_i^p(\cdot \mid t_{k+1}^i), y_i^a(\cdot \mid t_{k+1}^i), y_{-i}^a(\cdot \mid t_{k+1}^i)\right) \\ &= \sum_{k=0}^{N_p-2} l_i\left(y_i^*(k+1|t_{k+1}^i), u_i^*(k+1|t_{k+1}^i), y_i^*(k+1|t_{k+1}^i), y_{-i}^*(k+1|t_{k+1}^i)\right) \end{aligned} \tag{30}$$

Equation 30 is adjusted by *Equation 25* and *Equation 26* to the summation range:

$$V_i(t_{k+1}^i) \le \sum_{k=1}^{N_p-1} l_i\left(y_i^*(k \mid t_k^i), u_i^*(k \mid t_k^i), y_i^*(k \mid t_k^i), y_{-i}^*(k \mid t_k^i)\right) \tag{31}$$

Subtracting $J_i^*(t_k^i)$ from *Equation 31* yields:

$$\begin{aligned} V_i(t_{k+1}^i) - V_i(t_k^i) &\le \sum_{k=1}^{N_p-1} l_i\left(y_i^*(k \mid t_k^i), u_i^*(k \mid t_k^i), y_i^*(k \mid t_k^i), y_{-i}^*(k \mid t_k^i)\right) \\ &- \sum_{k=0}^{N_p-1} l_i\left(y_i^*(k \mid t_k^i), u_i^*(k \mid t_k^i), y_i^a(k \mid t_k^i), y_{-i}^a(k \mid t_k^i)\right) \\ &= -l_i\left(y_i^*(0 \mid t_k^i), u_i^*(0 \mid t_k^i), y_i^*(1 \mid t_k^i), y_{-i}^*(1 \mid t_k^i)\right) + \sum_{k=1}^{N_p-1} \delta_i \end{aligned} \tag{32}$$

where the disturbance term is:

$$\delta_i = \sum_{j \in \mathbb{N}_i} \left\|y_i^*(k \mid t_k^i) - y_j^*(k \mid t_k^i)\right\|_{G_i}^2 - \sum_{j \in \mathbb{N}_i} \left\|y_i^*(k \mid t_k^i) - y_j^a(k \mid t_k^i) - \tilde{d}_{i,j}\right\|_{G_i}^2 - \left\|y_i^*(k \mid t_k^i) - y_i^a(k \mid t_k^i)\right\|_{F_i}^2 \tag{33}$$

By applying the triangle inequality, *Equation 33* can be upper bounded as:

$$\delta_i \le \sum_{i \in N_i} \| y_j^*(k \mid t_k^i) - y_j^a(k \mid t_k^i) \|_{G_i}^2 - \| y_i^*(k \mid t_k^i) - y_i^a(k \mid t_k^i) \|_{F_i}^2 \tag{34}$$

From *Equations 31–34*, the following holds for a single vehicle node at time t_k^i:

$$V_i(t_{k+1}^i) - V_i(t_k^i) \le -l_i(y_i^*(0 \mid t_k^i), u_i^*(0 \mid t_k^i), y_i^a(0 \mid t_k^i), y_{-i}^a(0 \mid t_k^i)) + \varepsilon_i \tag{35}$$

where $\varepsilon_i = \sum_{k=1}^{N_p-1} \delta_i(k)$.

By summing the difference terms for all vehicle nodes $i = 1 \sim N$, the variation rate of the overall Lyapunov function is:

$$\begin{aligned} V(t_{k+1}) - V(t_k) &= \sum_{i=1}^{N} \left[V_i(t_{k+1}^i) - V_i(t_k^i)\right] \\ &\le -\sum_{i=1}^{N} l_i\left(y_i^*(1 \mid t_k^i), u_i^*(0 \mid t_k^i), y_i^a(1 \mid t_k^i), y_{-i}^a(1 \mid t_k^i)\right) + \sum_{i=1}^{N} \varepsilon_i \end{aligned} \tag{36}$$

To ensure a monotonic decrease of the Lyapunov function, *Equation 36* must remain strictly negative; that is, $\varepsilon_i \le 0$, with F_i and G_i satisfying the following condition.

$$F_i \ge \sum_{j \in \mathbb{N}_i} G_j, \forall i \in \{1, \cdots N\} \tag{37}$$

Finally, the entire vehicle platoon is asymptotically stabilised, as demonstrated by Lyapunov stability.

5. SIMULATION RESULTS

To verify the effectiveness of the proposed bandwidth-aware sigmoid event-triggered adaptive DMPC, this section presents simulation results based on real vehicle parameters under the MATLAB platform. In the simulation, the platoon is formed with one leader (vehicle 0) and seven followers (vehicles 1–7), with an inter-vehicle spacing of $d_{i-1,i} = 10\ m$. The information flow topologies considered are PF and PLF.

The simulation is conducted under acceleration and deceleration scenarios. Based on the parameters of a typical passenger vehicle, the simulation settings are as follows: the inertial lag of longitudinal dynamics (τ_i), aerodynamic drag coefficient ($C_{A,i}$) and tire radius ($r_{w,i}$) are assumed to have a linear relationship with vehicle mass (m_i), as listed in *Table 4*. The weighting matrices in DMPC influence both platoon performance and stability. F_i and G_i affect inter-vehicle coordination, R_i penalises deviations of the control input from the equilibrium, and Q_i determines the tracking accuracy with respect to the leader. To highlight the effects of the proposed method, identical weighting matrices F_i , G_i and R_i are assigned to all vehicles, as shown in *Table 5*, to eliminate the influence of weighting variations. The trajectory of the lead vehicle is defined by *Equation 38*.

Table 4 – Vehicle parameters in the platoon

Vehicle index	$m_i\ (kg)$	$\tau_i\ (s)$	$C_{A,i}\ (N \cdot s^2 \cdot m^{-2})$	$r_{W,i}\ (m)$
1	1035.71	0.52	0.99	0.30
2	1849.13	0.74	1.16	0.38
3	1939.99	0.78	1.16	0.37
4	1677.74	0.71	1.11	0.38
5	1753.74	0.71	1.14	0.36
6	1742.13	0.73	1.12	0.35
7	1392.23	0.62	1.06	0.34

Table 5 – DMPC weighting factors

Weights	PF	PLF
F_i	$F_i = diag(10,\cdots,10), i \in \mathcal{N}$	$F_i = diag(10,\cdots,10), i \in \mathcal{N}$
G_i	$G_1 = 0,$ $G_i = diag(5,\cdots,5), i \in \mathcal{N}\backslash\{1\}$	$G_1 = 0,$ $G_i = diag(5,\cdots,5), i \in \mathcal{N}\backslash\{1\}$
Q_i	$Q_1 = diag(10,\cdots,10),$ $Q_i = 0, i \in \mathcal{N}\backslash\{1\}$	$Q_i = diag(10,\cdots,10), i \in \mathcal{N}\backslash\{1\}$
R_i	$R_i = diag(1,\cdots,1), i \in \mathcal{N}\backslash\{1\}$	$R_i = diag(1,\cdots,1), i \in \mathcal{N}\backslash\{1\}$

$$a_0 = \begin{cases} 2m/s^2, & 2 \le t \le 3 \\ -1m/s^2, & 5 \le t \le 6 \\ 0 & \text{otherwise} \end{cases} \tag{38}$$

To evaluate the bandwidth-aware sigmoid threshold event-triggered mechanism within the adaptive horizon DMPC framework, the communication triggering frequencies of vehicles under different bandwidth parameters are compared. Once the triggering condition is met, vehicle i transmits its state to its follower; the last vehicle (7th) only receives information from its predecessor. *Figure 5* presents the communication triggering times and intervals under the PF topology for three bandwidth states, α=0 (busy), 0.5 (moderate) and 1 (idle). When $\alpha = 0$, bandwidth congestion reduces the triggering frequency and transmitted data volume, with a maximum interval of 1 second. In contrast, when $\alpha = 1$, sufficient bandwidth enables more frequent state updates and faster information exchange.

Comparison of the simulation results under these three bandwidth conditions reveals the following: under bandwidth congestion, the proposed bandwidth-aware event-triggered mechanism reduces the triggering

frequency, leading to slightly increased average spacing between vehicles. Nevertheless, the spacing deviations remain within safe limits, ensuring smooth platoon motion and satisfactory tracking accuracy. Conversely, with sufficient bandwidth, higher communication frequency allows for tighter spacing control and further improves tracking accuracy. These results demonstrate that the bandwidth-aware event-triggered mechanism effectively balances communication efficiency and platoon stability, ensuring both safety and tracking performance under varying bandwidth conditions.

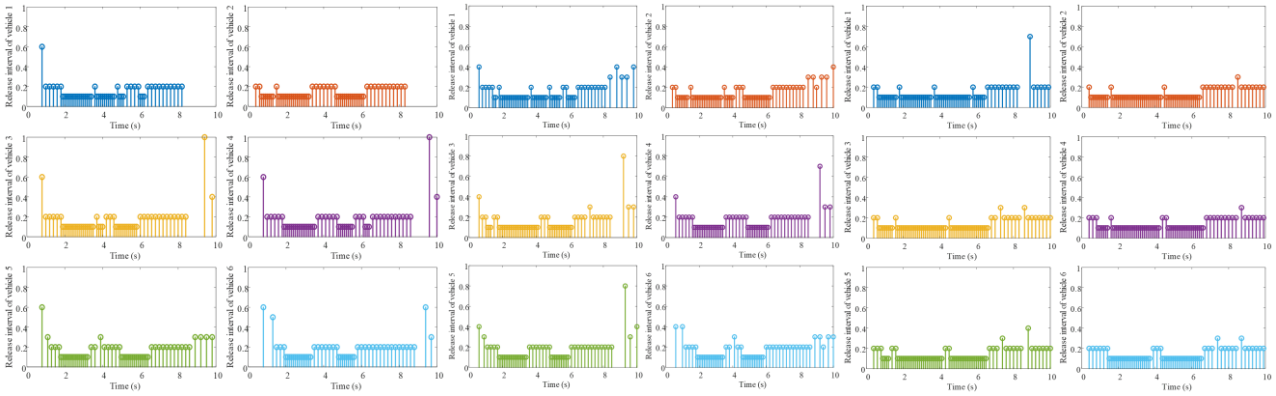

(a) *(b)* *(c)*

Figure 5 – Event-triggered communication behaviour of follower vehicles under different α values in PF topology: a) Triggering behaviour of each vehicle when $\alpha = 0$; b) Triggering behaviour of each vehicle when $\alpha = 0.5$; c) Triggering behaviour of each vehicle when $\alpha = 1$

Under acceleration and deceleration scenarios, the proposed mechanism is compared to the method presented in [15] in terms of communication efficiency. *Figure 6* compares the average triggering (i.e. communication) frequencies. The results demonstrate that the proposed algorithm significantly reduces communication frequency under both topologies, thereby conserving controller communication resources: approximately 16.4% under the PF topology and 18.7% under the PLF topology. This effectively alleviates the pressure induced by limited communication resources in the control system.

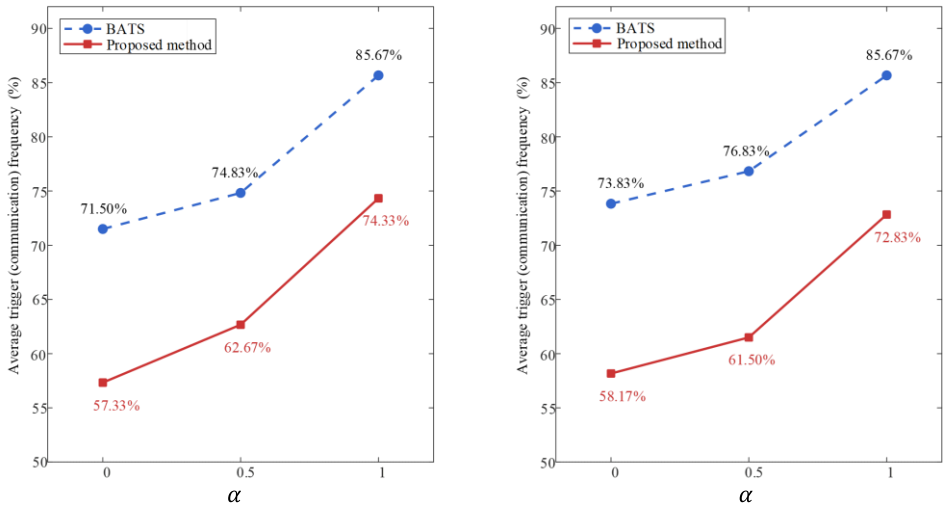

(a) *(b)*

Figure 6 – Comparison of average triggering (communication) frequency in the vehicle platoon: a) Average triggering (communication) frequency under PF topology; b) Average triggering (communication) frequency under PLF topology

Figure 7 illustrates that, under $\alpha = 0.5$, the proposed fuzzy adaptive-horizon DMPC reduces N_p from 20 to 10, compared to the fixed-horizon DMPC in [9]. As shown in *Table 6*, under the PF topology, the adaptive controller achieves an average computation time of 32.64 seconds, representing a 12.0% reduction compared to the fixed-horizon controller (37.09 seconds). Under the PLF topology, the adaptive approach achieves an average computation time of 32.88 seconds, representing a 20.45% reduction in computation time compared to the fixed-horizon case.

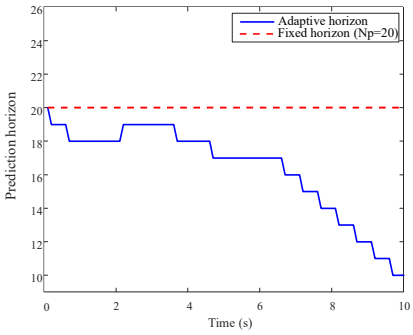

Figure 7 – Trend of prediction horizon variation ($\alpha = 0.5$)

Table 6 – Total DMPC processing time for 7 vehicles

Communications topology	Fixed prediction horizon	Adaptive prediction horizon		
		$\alpha = 0$	$\alpha = 0.5$	$\alpha = 1$
PF	37.09s	32.08s	32.70s	33.13s
PLF	41.33s	33.37s	33.28s	32.00s

To demonstrate the proposed approach's ability to maintain ideal platoon tracking under different topologies and communication conditions, simulations were conducted with $\alpha = 0.5$. The results are presented in *Figure 8*. *Figures 8a and 8b* indicate that the longitudinal velocities of following vehicles rapidly and smoothly track the lead vehicle's reference trajectory without overshoot. *Figures 8c and 8d* present the time-varying accelerations, confirming that the event-triggered strategy achieves the desired control objectives. *Figures 8e and 8f* illustrate the spacing errors relative to the lead vehicle, demonstrating that the longitudinal tracking errors of the following vehicles remain small, with a maximum spacing error of only 0.15 meters.

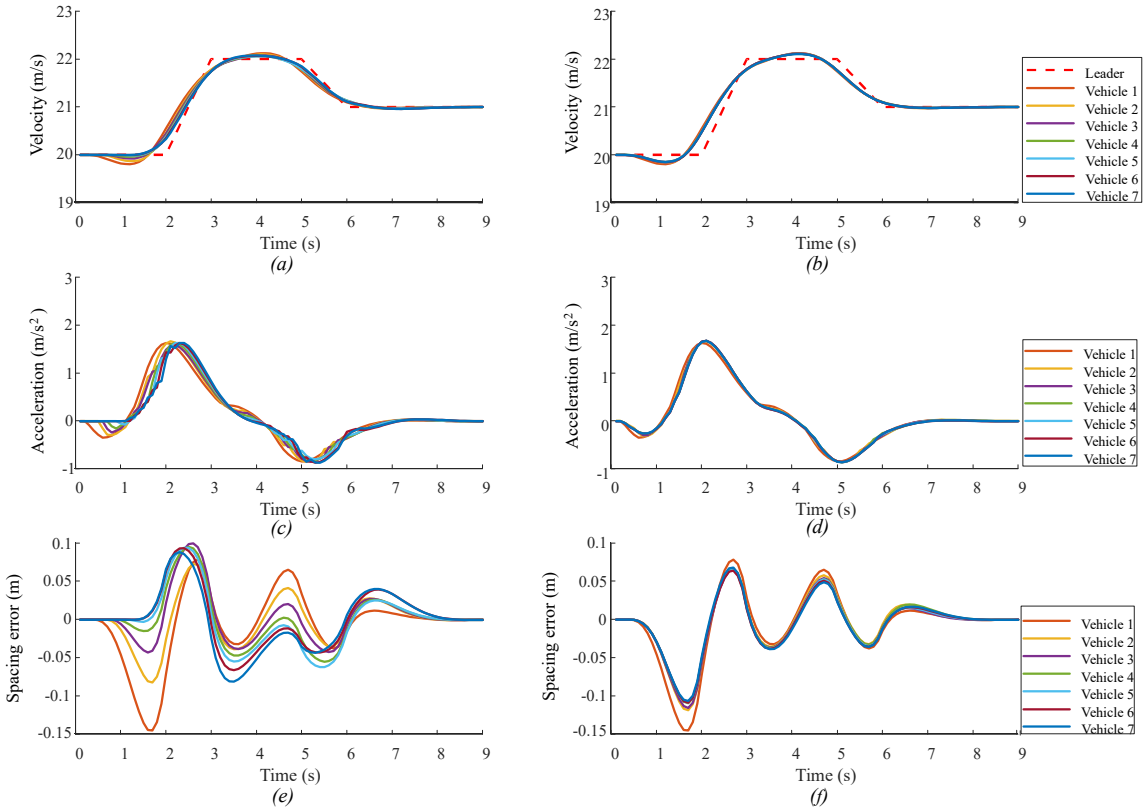

Figure 8 – Platoon state responses under PF and PLF topologies with $\alpha = 0.5$*: a) Vehicle speed variation under PF topology; b) Vehicle speed variation under PLF topology; c) Acceleration variation under PF topology; d) Acceleration variation under PLF topology; e) Spacing error with lead vehicle under PF topology; f) Spacing error with lead vehicle under PLF topology*

6. CONCLUSION

To address the challenges of limited bandwidth and computational constraints in heterogeneous vehicle platoons, this paper proposes a bandwidth-aware event-triggered adaptive DMPC method. While maintaining control performance, the method achieves dual optimisation of communication frequency and computational load in DMPC. Specifically, an event-triggered mechanism is designed to integrate bandwidth status and vehicle state errors via a sigmoid threshold function. This mechanism enables dynamic adjustment of data transmission triggering conditions and effectively reduces the data transmission frequency within the platoon. Furthermore, fuzzy rules constructed from the system's maximum position and velocity errors are employed to adaptively adjust the prediction horizon, thereby reducing computational complexity. Finally, simulations with one lead vehicle and seven following vehicles under acceleration and deceleration scenarios demonstrate the efficacy of the proposed approach. The results indicate that the method ensures platoon tracking performance while conserving communication and computational resources.

ACKNOWLEDGEMENTS

This research was funded by the Guangxi Key Laboratory of Automobile Components and Vehicle Technology (2023GKLACVTZZ07).

REFERENCES

[1] Zhang R, et al. The innovation effect of intelligent connected vehicle policies in China. *IEEE Access*. 2022;10:24738-24748. DOI: 10.1109/ACCESS.2022.3155167.

[2] Shao Y, Sun Z. Eco-approach with traffic prediction and experimental validation for connected and autonomous vehicles. *IEEE Transactions on Intelligent Transportation Systems*. 2020;22(3):1562-1572. DOI: 10.1109/TITS.2020.2972198.

[3] Oliveira R, et al. Co-Design of consensus-based approach and reliable communication protocol for vehicular platoon control. *IEEE Transactions on Vehicular Technology*. 2021;70(9):9510-9524. DOI: 10.1109/TVT.2021.3101489.

[4] Hou J, et al. Large-scale vehicle platooning: advances and challenges in scheduling and planning techniques. *Engineering*. 2023;28:26-48. DOI: 10.1016/j.eng.2023.01.012.

[5] Moode S N, Soriguera F. Microscopic modeling of connected autonomous vehicles platooning: stability and safety analysis. *Transportation Research Procedia*. 2023;71:260-267. DOI: 10.1016/j.trpro.2023.11.083.

[6] Wu J, Qu X. Intersection control with connected and automated vehicles: A review. *Journal of Intelligent and Connected Vehicles*. 2022;5(3):260-269. DOI: 10.1108/JICV-06-2022-0023.

[7] Wang D, et al. Online model predictive control for energy-saving train operation in passenger-freight mixed lines. *Promet-Traffic&Transportation.* 2024;36(6):1039-1053. DOI: 10.7307/ptt.v36i6.589.

[8] Peng Y, et al. Distributed model predictive control for unmanned aerial vehicles and vehicle platoon systems: a review. *Intelligence & Robotics*. 2024;4(3):293-317. DOI: 10.20517/ir.2024.19.

[9] Zheng Y, et al. Distributed model predictive control for heterogeneous vehicle platoons under unidirectional topologies. *IEEE Transactions on Control Systems Technology*. 2017;25(3):899-910. DOI: 10.1109/TCST.2016.2594588.

[10] Feng Y, et al. Distributed MPC of vehicle platoons with guaranteed consensus and string stability. *Scientific Reports*. 2023;13(1):10396. DOI: 10.1038/s41598-023-36898-4.

[11] Wei H, Zhang H, Kamal A I H, et al. Ensuring secure platooning of constrained intelligent and connected vehicles against Byzantine attacks: A distributed MPC framework. *Engineering*. 2024;33:35-46. DOI: 10.1016/j.eng.2023.10.007.

[12] Yang R, et al. Distributed MPC multi-objective optimization control for commercial vehicle platoon under time delay conditions. *Automotive Engineering*. 2025;47(03):418-429. DOI: 10.19562/j.chinasae.qcgc.2025.03.004.

[13] Bansal K, Mukhija P. Event-triggered control of vehicular platoon system with time-varying delay and sensor faults. *Proceedings of the Institution of Mechanical Engineers, Part D: Journal of Automobile Engineering*. 2020;234(14):3362-3372. DOI: 10.1177/0954407020932676.

[14] Ge X, et al, Dynamic event-triggered scheduling and platooning control codesign for automated vehicles over vehicular ad-hoc networks. *IEEE/CAA Journal of Automatica Sinica*. 2022;9(1):31-46. DOI: 10.1109/JAS.2021.1004060.

[15] Han Q, et al. Bandwidth-aware transmission scheduling and event-triggered distributed mpc for vehicle platoons. *2022 41st Chinese Control Conference (CCC). IEEE*. 2022:5532-5538. DOI: 10.23919/CCC55666.2022.9901846.

[16] Du C, et al. Hierarchical Event-triggered platoon control for heterogeneous connected vehicles subject to actuator uncertainties and non-zero inputs. *IEEE Transactions on Intelligent Transportation Systems*. 2025;26(1):235-253. DOI: 10.1109/TITS.2024.3480929.

[17] Zhang J, Xia H, Ma G. Output-constrained fixed-time coordinated control for multi-agent systems with event-triggered and delayed communication. *Information Sciences*. 2024;659:120086. DOI: 10.1016/j.ins.2023.120086.

[18] Zhang P, et al. Sigmoid-like event-triggered security cruise control under stochastic false data injection attacks. *Processes*. 2022;10(7):1326. DOI: 10.3390/PR10071326.

[19] Xie H, et al. High minimum inter-execution time sigmoid event-triggered control for spacecraft attitude tracking with actuator saturation. *IEEE Transactions on Automation Science and Engineering*. 2023;20(2):1349-1363. DOI: 10.1109/TASE.2022.3179896.

[20] Lin X, Tang Y, Zhou B. Improved model predictive control path tracking strategy based an online updating algorithm with cosine similarity and a horizon factor. *IEEE Transactions on Intelligent Transportation Systems*. 2022;23(8):12429-12438. DOI: 10.1109/TITS.2021.3114060.

[21] Li Y, et al. Path planning and path tracking for autonomous vehicle based on MPC with adaptive dual-horizon-parameters. *International Journal of Automotive Technology*. 2022;23(5):1239-1253.

[22] Liu H, Sun J, Cheng K W E. A two-layer model predictive path-tracking control with curvature adaptive method for high-speed autonomous driving. *IEEE Access*. 2023;11:89228-89239. DOI: 10.1109/ACCESS.2023.3306239.

[23] Wang T, Kang Y, Li P F. Adaptive event-triggered distributed model predictive control for tracking consensus of multiagent systems. *Scientia Sinica (Technologica)*. 2023;53(11):1885–1894. DOI: 10.1360/SST-2021-0379.

[24] Wang P, Ren X, Zheng D. Event-triggered asynchronous distributed model predictive control with variable prediction horizon for nonlinear systems. *International Journal of Robust and Nonlinear Control*. 2023;33(6):3764-3789. DOI: 10.1002/rnc.6595.